UNIVERSITY OF CALIFORNIA,

IRVINE

Fog Harvesting with Cylindrical Fog Cage

THESIS

Submitted in partial satisfaction of the requirements
For the degree of

MASTER OF SCIENCE

in Mechanical and Aerospace Engineering

by

Ronald K. Kwok

Thesis Committee:

Associate Professor Yoonjin Won, Chair

Assistant Professor Penghui Cao

Professor Yun Wang

2022

DEDICATION

To

my parents, friends, and colleagues

in recognition of their worth

and unconditional support.

TABLE OF CONTENTS

LIST OF FIGURES

LIST OF TABLES

ACKNOWLEDGEMENTS

I would like to express my sincerely gratitude to my thesis committee chair- Professor Yoonjin Won, for her invaluable advice, immense knowledge, and plentiful experience had guided me through my research. Without her counsel, this thesis would not have been possible.

I would like to thank our research partner Mansur Abahusayn, PhD, his experience, knowledge, and pursuit in fog harvesting technology had been the foundation of this research project.

I would like to acknowledge my lab mates, Jonggyu Lee and Cheng-Hui Lin, for their key mentorship and assistance in constructing the fog chamber, fabricating the hydrophobic and hydrophilic copper surface, acquiring contact angles, acquiring scanning electron microscopy images.

This work received financial support from the Water Energy Nexus (WEX) Center at the University of California, Irvine.

ABSTRACT OF THE THESIS

Fog Harvesting with Cylindrical Fog Cage

By

Ronald K. Kwok

Master of Science in Mechanical and Aerospace Engineering

University of California, Irvine, 2022

Associate Professor Yoonjin Won, Chair

Worsening water scarcity due to global warming and frequent La Niña episodes presses countries to develop diverse water resources. Without consuming much energy, atmospheric fog water can be harvested as an environmentally friendly alternative water resource. Different designs and complexities of fog harvesters have been produced. From simple but economical fog harvesting mesh and harps to complex but sophisticated bio-mimicking and -inspiring fog harvesting structures, each fog collector is designed to be more efficient than preceding models. In this study, we propose an alternative fog collector design in a fully radial symmetric cylindrical geometry for versatility. The design provides a stable aerodynamic and deposition efficiency according to the fog harvesting efficiency mode. Therefore, it can maximize its efficiency regardless to change in the wind direction. We also examine the effectiveness of certain design improvements such as layered collector's surface and wettability modification on improving the collector's efficiency. We test the collector in a controlled custom fog chamber, in which we measure and record its performance for evaluation. The data are used for discussing design optimization, and further works for versatile fog harvesting.

CHAPTER 1: INTRODUCTION

A sustainable source of fresh water is indispensable to social and economic development of civilizations. Unfortunately, inhabitants from developing regions often find themselves suffering from water scarcity due to arid climate, topographical constrains, inadequate infrastructure, pollution, etc. [1, 2]. To alleviate water scarcity and support sustainable developments around the globe, the United Nation has been advocating creative exploitation of unconventional water resources [3]. With specialized processes and technologies, scientists are able to extract fresh water out of some readily available unconventional resources which include, but not limited to, waste water, brackish water [4, 5] , offshore ground water [6], and atmospheric moisture [7]. Of the few mentioned, the capture of atmospheric moisture, specifically fog harvesting, has seen increasing adaptation in small rural communities where fog events are frequent. The most appealing aspects of the technology is the low installation and maintenance costs [8]. Since the 90's, fog harvesting projects piloted by non-profit entities have been generating drinking water for the local population as well as irrigation for the farmlands in central America, southern America, eastern Africa, southern Asia, etc [9, 10].

1.1 Diversification of Freshwater Supply with Unconventional Water Resources

A diversified water resources can safeguard local water supply, providing a safety net for the locals' water demand against any adverse situations. Water scarcity has dire consequences to the local inhabitant, economy, and environment. For example, inadequate irrigation results in crop failure, inevitably leading to food shortage that causes inflation in food prices and malnutrition among the impoverished communities. Meanwhile, the combustible dried vegetation will become the fuel of impending wildfire. The current rapid climate change driven by global warming is exacerbating water scarcity in arid regions. Long lasting droughts, severe heat waves, and ravaging

wildfires further diminish the reserves in the conventional water resources, e.g., surface water, ground water, and frozen water. To increase freshwater supply, various processes are developed to extract freshwater from unconventional resources that were once considered less practical. Among different resources, the reclamation of wastewater and desalination of brackish water and seawater are the most common [11]. Reclaimed wastewater is used in multiple ways, e.g., rebottling as drinking water, reusing for agricultural irrigation, and recharging into surface or ground water [12]. At a production rate of 209 cubic meters per year per capita in North America and 49 cubic meters per year per capita for the world's average [13], wastewater is the second largest accessible unconventional water resources. However, people have a low acceptance in using reclaimed water for close-to-body uses due to concerns in personal hygiene despite the advancements in filtration processes [14]. On the other hand, desalination turns seawater and brackish water into freshwater by thermal distillation or membrane desalination. Thermal distillation, the primary method of the two, produces much cleaner water at 10ppm. Although desalination receives better public acceptance than reclamation, it consumes at least 10 times the energy required by a reverse osmosis system used in treating wastewater. The cost of water by desalination can be as high as 1 US Dollar per cubic meter [15]. In comparison, the U.S. Department of Energy accounted a national average commercial water rate of 86 cents per cubic for 2016 [16].

1.2 Atmospheric Water and Fog Harvesting

The third and the most accessible unconventional water resource is atmospheric water. Atmospheric water refers to the moisture within the earth's atmosphere in the form of water vapor or microdroplets. Since this water resource is available anywhere, it becomes the saving grace for remote communities that lacks alternatives. Extraction of atmospheric water is currently achieved by two processes: dew harvesting and fog harvesting. In dew harvesting, water vapor is condensed

into its liquid phase inside a heat exchanger and the condensate is collected for use. Mobile atmospheric water condenser, such as the ones developed by Watergen [17], are used in humanitarian missions to produce clean drinking water on the go. In fog harvesting, the water is extracted from air by passive capture of the airborne microscopic water droplets which is commonly referred as fog. It differs from dew harvesting that no thermal exchange or change of phases occurs during the process. Fog can often be observed carried by the wind traveling close and parallel to the ground. Although fog is a common atmospheric phenomenon, dense harvestable fog is limited. Majority of feasible sites are located near lakes, ocean shores, or in the mountains [7].

It has always been a challenge and a topic of interest for researchers to increase the harvest of fog water. Volumes of research are spent on designing different geometries, materials, and surface morphology for fog collectors to increase their efficiencies. Beginning with the proposal of standard fog collectors using Raschel mesh in 1994 [18], the mesh design has been continually studied and refined by switching the mesh material, fining the fiber, adjusting the porosity, alternating the surface wettability, etc. [19, 20, 21, 22] A derivative of the mesh design is the fog harp which reduces pinned droplets by foregoing the longitudinal threads which provide support and extra area for wetting [23, 24]. In addition to inventing artificial structures, researchers have also drawn inspirations from nature to develop unique fog collectors. Park and Kim engineered a three dimensionally structured flexible hybrid fog collector mimicking the shell of a Namib desert beetle [25]. Inspiration drawn from spider webs leads to the development of the micro-cavity fiber by Tian Y. et al. [26]. Meanwhile, the biological water channels on the leaves of Dryopteris Marginata and other fog collecting grasses are studied and artificially replicated into hydrophilic nanochannels to assist water delivery on collectors' surface [27].

Rather than attempting new designs for breaking records, we do so to improve the versatility of existing fog collectors' concepts without costing their performance. In the following, we introduce a new cylindrically shaped fog collector. We will first review the design considerations for improving fog harvesting., then discuss the design and aspects for the cylindrical fog collector. Afterward, we will be evaluating the design by measuring its performance in terms of the collection efficiency through experimentation. In addition, we will also be studying the impact of surface wettability modification on the collection efficiency.

CHAPTER 2: DESIGN CONSIDERATIONS FOR FOG COLLECTOR

In this chapter, we will be reviewing a few design considerations including shape parameters, geometric parameters, and surface wettability for improving fog harvesting efficiency.

2.1 Droplet Deposition

Deposition of the airborne fog water microdroplets onto an obstacle occurs during inertia impaction [28, 29]. As a microdroplet impacts a solid obstacle in its path, it decelerates due to the friction force by the no-slip boundary condition until it loses all momentum and sits on the obstacle's surface.

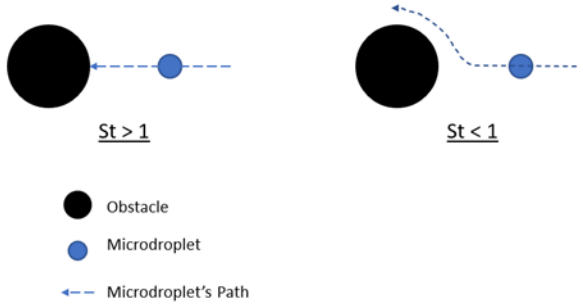

Figure 2.1 The likely path of microdroplets encountering an obstacle based on Stokes Number.

The likelihood of inertia impaction occurring is predicted by the dimensionless Stokes Number, St,

$$St = \frac{2\rho_{fog} u_{\infty} r_{fog}^2}{9\mu_{air} l_0} \qquad (2.1)$$

where ρ_{fog}, r_{fog}, μ_{air}, u_{∞}, l_0 are respectively the microdroplet's density, microdroplet's radius, the air's dynamic viscosity, the unperturbed wind speed, and the obstacle's characteristic length. Microdroplets with small Stokes Number (St < 1) are less dominated by their own inertia and therefore follow the air's path to circumvent the obstacle, resulting in no collision. At St > 1, the microdroplet's inertia dominates and the droplet is less responsive to abrupt change in the airflow, causing it to collide with the obstacle [30]. The microdroplets deposited on the obstacle's surface coalesce with each other or with newly arriving microdroplets to grow into critical mass and fall in the presence of gravity. Observed in *equation 2.1*, we can control the Stokes Number by

adjusting l_0 but the other variables are governed by nature. In the case of a cylindrical obstacle, e.g. a piece of wire or tube, the characteristic length measures the outer diameter. The smaller the tube diameter; the better chance of guaranteeing an inertia impaction

2.2 Aerodynamics and Directional Dependency

Beside droplets deposition, efficiency of a fog collect is also affected by its aerodynamics, which in turns depends on the collector's shade coefficient (SC). According to Rivera [31], shade coefficient accounts for the portion of the collector's area that is capable of capturing droplets. On the collector, the capable area is occupied by obstacles to the fog. Alternatively, SC can be calculated from its inverse, the free area ratio (*f*).

$$SC = 1 - f \quad \text{and} \quad f = \frac{A_{op}}{A_{screen}} \tag{2.2}$$

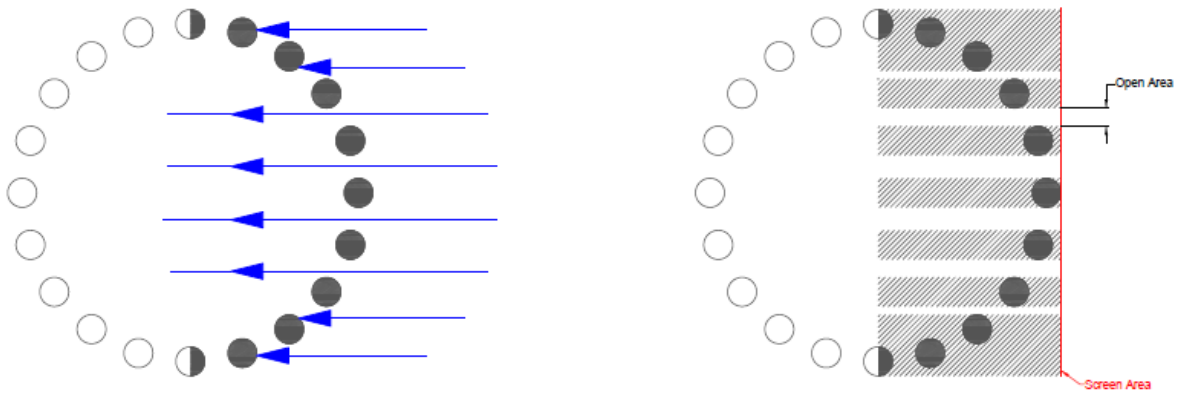

Figure 2.2 Illustration for measuring the screen and open area with respect to the fog stream.

A_{op} is the total opening area on the collector, and A_{screen} is the collector's screen area. As mentioned previously, the wind seeks to circumvent all obstacles in its path. The change to the flow trajectory is felt by each neighboring layer of air molecules until some distance away from the obstacle. Such

distance increases at the presence of larger and less permeable obstacles (a SC approaching 1), which corresponds to more microdroplets being carried by the wind away from the collector. On another hand, highly permeable and small obstacles (a SC of approaching 0) present limited surface area to capture and collector the microdroplets. More importantly, the collector's shade coefficient may change according to the wind direction. When the wind comes at a steep angle, a fog harvesting mesh or harp will find its capable areas overlapped, increasing the SC.

2.3 Layered Fog Collector

A layered structure increases the probability of microdroplets capture. At the first layer, some microdroplets will escape by either passing through the gaps in the layer or by re-entrainment. Re-entrainment occurs when the aerodynamic drag force acting on a droplet is greater than the tension at the liquid-solid interface, which then causes the droplet to peel off from the surface where it once settled. In a layered structure, subsequent layers provide addition surface for the escaped droplets to collide with. The effectiveness of layer collectors has been previously explored by Azeem et al. [32] using harp type collectors. They reported that the double-layered harp (SC = 0.17 per layer) increased the collector's water production by 85% as compared to a single-layered. Water Droplets Removal and Wettability Modification

2.4 Water Drainage and Wettability

Improving fog harvesting by facilitating droplets removal is made possible by development of new technology in chemistry and microstructure engineering. Surface film coating and microstructure fabrication are often employed to modify the surface's wetting characteristic The wettability of the collectors' surface influences the mobility of the deposited water droplets.

Wettability is measured by the static contact angle, Θ_s, governed by the classic Young-Dupre's equation for smooth surfaces:

$$cos\theta_s = \frac{\gamma_{SV}-\gamma_{SL}}{\gamma_{LV}} \qquad (2.3)$$

and Wenzel's equation for rough surfaces:

$$cos\theta_s^* = rcos\theta_s \qquad (2.4)$$

Where Y_{SV}, Y_{SL}, and Y_{LV} are the surface tensions at the liquid-solid, solid-vapor, and liquid-vapor interface; Θ_s* is the static contact angle on rough surface, and r is the roughness ratio between the actual and the projected surface area. A surface is hydrophobic if its Θ_s* is greater than 90° and superhydrophobic for 150° and greater. Oppositely, a surface is hydrophilic if its Θ_s* is lower than 90° and superhydrophilic for 10° or lower. Since r is always larger or equal to 1, rough surfaces will either increase the hydrophobicity of a hydrophobic surface or increase hydrophilicity of a hydrophilic surface.

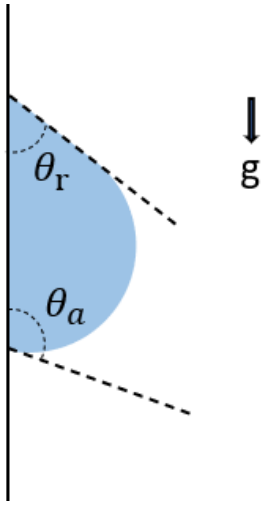

Figure 2.3 The receding and advancing contact angle of a typical droplet on vertical surface.

The pinning force, f_{pin}, acting on a droplet is caused by the contact angle hysteresis, and is equal to the critical weight of the droplet at the onset of droplet movement:

$$f_{pin} \approx \pi r_d \gamma_{SL}(cos\theta_r - cos\theta_a) \approx \rho_d V_{cr} g \qquad (2.5)$$

Where r_d and ρ_d is the droplet radius and density, Θ_r *and* Θ_a are the receding and advancing contact angles, V_{cr} is the critical volume of the droplet, and g is the gravitational acceleration constant. At the onset of droplet shedding, the critical weight of the droplet equals to f_{pin}. A study

on fog harvesting with hydrophobic surfaces conducted by Seo et al. [33] has shown that hydrophobic and superhydrophobic surfaces increases water collection by 2.70% and 8.11% respectively with thrice the droplets shedding rate as compared to an unmodified neutral surface. In current time, surfaces with engineered wettability gradient or differential are popular in research related to bio-inspired and bio-mimicking fog collectors.

In the chapter, we introduce various influential design parameters for an efficient fog collector. They include the geometric parameters which affect droplet deposition and aerodynamics; shape parameters that depend on the wind direction; and surface wettability that changes the mobility and behavior of the droplets. Later, we will go through our design methodology to develop a cylindrical fog collector for versatility.

CHAPTER 3: THE CYLINDRICAL FOG CAGE DESIGN

In this chapter, we will be discussing our methodology to design a versatile cylindrical fog collector. The idea is to prototype a collector with stable efficiency despite unpredictable changes in its operation condition.

3.1 The Fog Harvesting Efficiency Model

The fog harvesting efficiency model is a powerful design tool to relate the efficiencies of a collector design to its geometric parameters. It redefines the collection efficiency, η_{col}, as a function of the shade coefficient and Stokes number. η_{col} is defined as the ratio of the usable water mass collected by the fog collector, m_w, to the potential liquid water content originally stored within the same volume of unperturbed fog.

$$\eta_{col} = \frac{m_w}{LWC \cdot u_\infty A \cdot \Delta t} \qquad (3.1)$$

where LWC is the liquid water content per volume (g/m^3) of the fog, A is the area (m^2) of the unperturbed fog flux upstream of the collector, Δt is the duration for the fog harvest in seconds. Later studies [31, 24] have shown that the collection efficiency is the product of the aerodynamic efficiency, η_a, and deposition efficiency, η_d.

$$\eta_{col} = \eta_a \eta_d \qquad (3.2)$$

η_a accounts for the fraction of fog impacting the impermeable surface of the collector, and is a function of the collector's shade coefficient, SC. Whereas η_d accounts for the fraction of droplets depositing onto the collector from the fog, and is a function of the Stokes Number.

$$\eta_a = \frac{SC}{1+(C_0/C_D)^{1/2}} \qquad (3.3)$$

$$\eta_d = \frac{St}{St+(\pi/2)} \quad (3.4)$$

$$C_0 = k_{Re}\left[1.3SC + \left(\frac{SC}{1-SC}\right)^2\right] \quad (3.5)$$

$$Re = \frac{2\rho_{air}u_\infty l_0}{\mu_{air}} \quad (3.6)$$

The drag coefficient, C_D, is a tabulated shape factor. The variable C_0 is the pressure drop coefficient and a function of SC corrected by an empirical correction factor, k_{Re}, based on the Reynolds number, Re. [19] The empirical formula for k_{Re} is displayed in the work by Shi et al. [24]

The operating environment for any fog collector is highly dynamic. Wind direction can change unexpectedly at common fog harvesting sites in the mountain or close to the shore. If we can remove shade coefficient's dependency on the wind direction, the aerodynamic efficiency will become a constant during operation because shade coefficient will also become a constant according to *equation 3.3 and 3.5*. Our solution is to build a fully radial symmetric collector.

3.2 A Fully Radial Symmetric Collector

The primary characteristic of the new fog collector is to be aerodynamically stable regardless of the wind direction parallel to the ground. Fully radial symmetric structures, e.g., cylinder, sphere, and spheroid, are best at reproducing a highly similar, or identical, shade coefficient from any radial direction. Incidentally, the symmetric shape also created a layered structure for fog harvesting. When picked up by the wind, the fog enters the structure from the front, then leaves in the back, traversing the collector twice. We decide to proceed with a cylindrical shape for the fog collector because it is less complicated to fabricate than a sphere or spheroid. It is also easier to build supports to stand on the ground or hang from above. For the porous collection surface, we reproduce the fog harp [24] on the cylinder but replace the wires with copper tubes to increase the

rigidity of the structure. As mentioned previously, the fog harp is more effective for shedding water droplets the mesh. The appearance of the cylindrical fog collector, as shown in *figure 1*.3, resembles a cylindrical cage, hence the name Cylindrical Fog Cage.

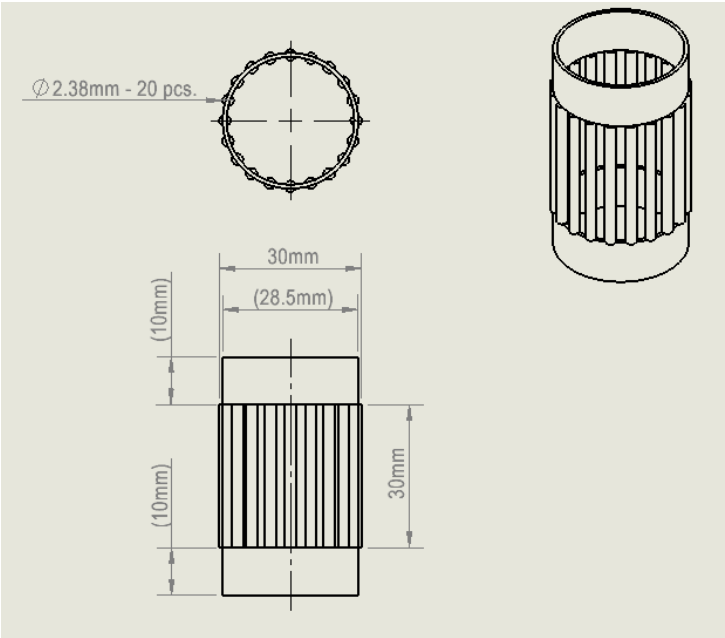

Figure 3.1 Schematic of the Cylindrical Fog Cage (CFC).

3.3 Stable Shade Coefficient and Aerodynamics

To confirm that the CFC's SC and aerodynamics is stable in any radial direction, we create an 3D model for the collector on SolidWorks2021 at 1:1 scale. We measure the screen and the total open area on the forward half of the CFC to calculate the SC. We rotate the model by 30 degrees, 45 degrees, and 60 degrees to simulate an equivalent change in the wind direction, and re-measure the areas to calculate the corresponding SC. Meanwhile, we also perform a computational fluid dynamic (CFD) analysis on the model using the flow simulation tool on SolidWorks (*figure 3.2e~3.2h*). The analysis uses an external flow with no boundary conditions on the computation domain. Fog is represented by highly saturated air (90% RH) at 20^{o}C and 1.0 atm with a wind speed of 1.1m/s. The CFC's surface is smooth and adiabatic. The mesh is generated automatically

using a global mesh size of 4mm x 3mm x 3mm (L x W x H) with level 1 refinement. Separation between neighboring flow trajectory grids is 2.0mm. For comparison, an equivalent fog harp with identical width (30mm) and similar pitch (4.6mm on the fog harp and 4.3mm on the CFC) is modeled in SolidWorks2021 with its SC calculated, and the model analyzed using SolidWorks' flow simulation under the same parameters (*figure 3.2a~3.2d)*. By the calculations and CFD results, the cylindrical fog cage's SC is largely unchanged, and the separation between the flow trajectories across the cylinder is more stable than the fog harp throughout the rotation, which suggest the aerodynamics, and the aerodynamic efficiency, on the CFC is likely unaffected by the rotation.

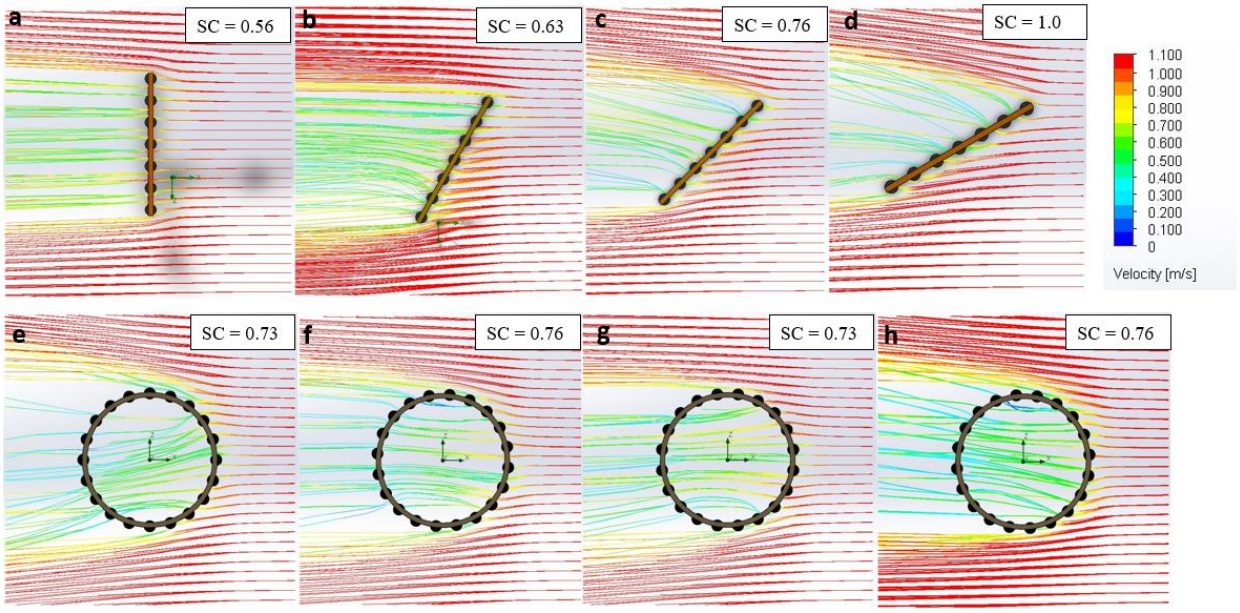

Figure 3.2 Simulated flow trajectories across a fog harp and a CFC. The fog's flow path, as represented by the flow trajectories from the CFD analysis, across the fog harp is displayed in (a)~(d), and the cylindrical fog cage is displayed in (e)~(h). The angle of rotation applied to the collectors are 0^o in (a) and (e), 30^o in (b) and (f), 45^o in (c) and (d), 60^o in (d) and (h). The corresponding measured shade coefficient is placed on the top right corner of each figure. The separation between flow trajectories after the fog harp increases with the angle of rotation, but the separation across the CFC remains the same.

3.4 Surface Wettability Modification

Water drainage is equally important to the deposition of droplets and aerodynamics of the structure. Pinned water droplets on the collector's surface is unusable, which corresponds to loss in collection efficiency. Since the pinning force on the water droplet is largely affect by the contact angles, i.e. the surface wettability, a modification is needed for changing the wetting characteristic of the collector's surface. With the chemicals that are readily available to us, installing nanostructures by oxidizing copper through solution immersion method [34], and depositing hydrophobic molecules through dip-coating are the least expensive and reliable methods to produce hydrophilic and hydrophobic surfaces.

CHAPTER 4: CFC Fabrication and Test System Construction

The fabrication of the CFC, procedure for surface wettability modifications by solution immersion or dip-coating method, and the construction of the test system for the fog harvesting experiment is detailed in this chapter.

4.1. CFC Fabrication

Each CFC is constructed by distributing the vertical columns between two cropper rings functioning as the top and base holders. The holders are cut from a copper pipe of 28 mm outer diameter (Mueller Industries MH10002) and their average height is approximately 10mm. The columns of the CFC are made with thin copper tubes of specific diameters distributed evenly between holders. To fix the columns at the specific position, notches are cut into the holders and the tubes are secured by twisted copper wires tied to the notches. The following copper tubes of specific ODs were purchased from McMaster Carr. and installed on the cage: 1.59mm(7190K51), 2.38mm(7190K52), 3.18mm(7190K54), 3.97mm(7190K53), 4.76mm(7190K55). Each tube is cut to 30mm in length from the original stock.

We fabricate eight CFCs with distinct SC by controlling either the columns' diameters or its quantity. The first set of 4 CFCs are limited to having only 10 columns, but the columns diameter varies between each CFC. The second set of another 4 CFCs are limited to 2.38mm diameter columns, but have different columns counts between them.

Figure 4.1 Side and Top view of a completed CFC made with bare copper tubes of 2.38mm diameter secured to the holders with twisted copper wires.

4.2. Surface Wettability Modifications

We modify the surface wettability of the CFC's columns by fabricating copper oxide nanostructures on the copper tubes surface with the solution immersion method. Each copper tube is turned superhydrophilic or superhydrophobic before being installed onto the CFC.

4.2.1 Hydrophilic Surface Modification

After cutting each copper tube into the specified length, we proceed to clean the copper tubes with the following procedure to remove any contaminants and oxidation on the copper surface:

i. Rinse in acetone ultrasonically for 30 seconds.

ii. Rinse in Deionized (DI) water for 10 seconds

iii. Immerse in HCl, 5% by volume, for 90 seconds.

iv. Rinse in DI water for 20 seconds.

v. Rinse in isopropyl alcohol for 10 seconds.

vi. Air-dry the copper tube and preheat it on a hotplate at 70°C for 30 seconds.

We then fully immerse the preheated copper tube in the oxidizing solution (0.1M $K_2S_2O_8$+ 2M $NaOH$ in DI water) for two minutes. After two minutes of immersion, the copper tube is

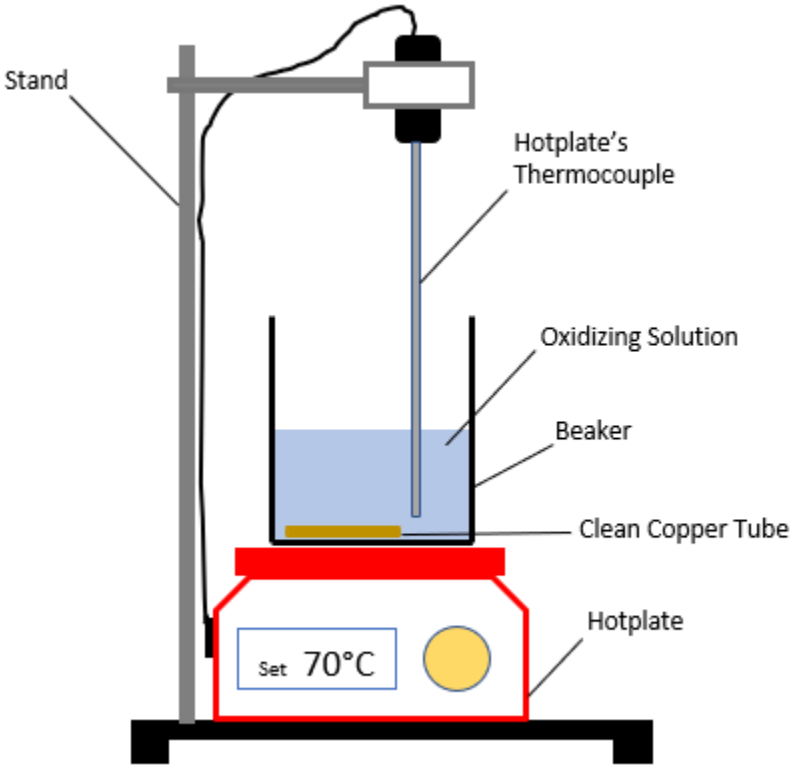

Figure 4.2 Fabrication set up for immersion method to oxidize the surface of a 30mm long copper tube.

removed from the oxidizing solution, and rinsed in DI water for 30 seconds and isopropyl alcohol for 10 second. At last, the hydrophilic copper tube is air-dried and ready to be installed onto the CFC.

4.2.2 Hydrophobic Surface Modification

To produce the hydrophobic copper tubes for the CFC, we apply a hydrophobic coating to the hydrophilic tubes to further functionalize the surface and reduce the surface energy. The selected coating solution is 5mM Dodecanoic acid ($C_{12}H_{24}O_2$ diluted with ethanol). The air-dried copper tubes are immersed in the coating solution for 30 minutes at room temperature. Afterward, the

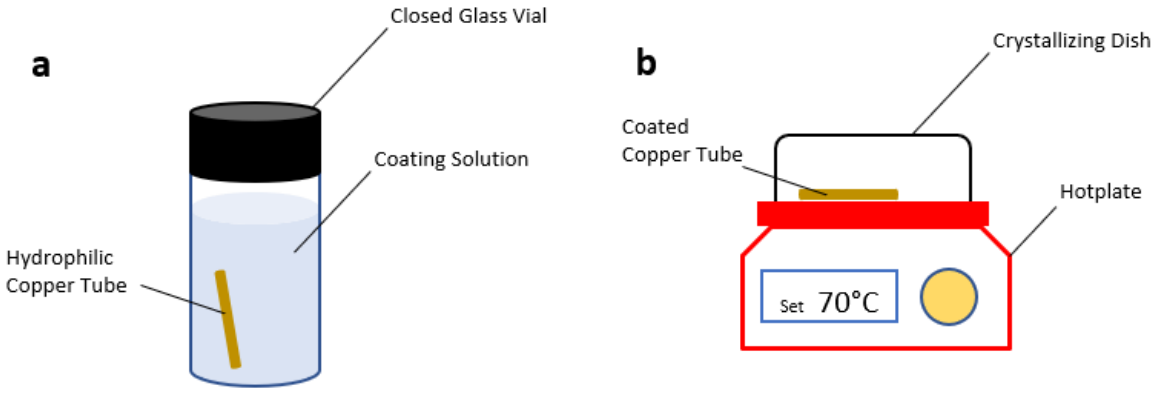

Figure 4.3 Fabrication set up for a) coating and b) baking procedures to create the hydrophobic copper tubes.

tubes are removed from the solution and baked on a hotplate, covered by a crystallizing dish, at 70°C for 30 minutes.

4.2.3 Validating Surface Wettability

The surface wettability of the copper tubes is validated by measuring the static contact angles on an equivalent flat surface using the sessile droplet method with a goniometer (MCA-3, Kyowa Interface Sciences). The equivalent flat surface is fabricated with the above procedures for hydrophilic and hydrophobic surface modifications on a flattened 1 cm X 1 cm Multipurpose 110 Copper Sheet (99.9% pure) purchased from McMaster-Carr. The goniometer dispenses a 15nL droplet of DI water at room temperature onto the sample by minimizing the gravity effect. The

droplet dynamic is captured by a high-speed camera at 5000 fps which enable us to measure the static contact angle from the images on a computer. Five measurements are taken individually for each sample at different locations and their average is reported. The averaged Θ_s from the hydrophobic surface is 165° and the hydrophilic surface is 9.9°, which shows superhydrophobicity and superhydrophilicity respectively.

4.3. Experimental Fog Chamber

An enclosed space with fog generation is needed for testing the CFC, so we build a custom test system (*figure 3.4*) with a 55 cm X 30 cm X 45 cm fog chamber made of clear acrylic sheets. Two circular openings of approximately 9 cm in diameter are cut on the fog chamber wall as the inlet and outlet for the fog stream. A computer fan locating at the outlets draws the fog out from the chamber into the ambient. The fog inlet is connected to the fog generator and air supply with acrylic and PVC pipes. Air is drawn from the ambient at 20℃ and 50% relative humidity (RH). The air supply is conditioned by a humidifier to increase the RH to 90%. The fog is generated by an ultrasonic humidifier (TaoTronics TT-AH009). The average fog generation rate is measured at 90 g/hr with an average droplet diameter of 7.5 μm. The fog mixes with air supply in the pipes, then enters the chamber through a channel of 30 mm inner diameter. The CFC is placed 1 cm away from the channel's exit, where a wind speed of 1.1 m/s is measured with a digital anemometer (Kritne HP-866B-APP). The fog water is drained into the custom 3D-printed sink and transferred to the containers for weighting.

At the beginning of each test, before activating the fog generator, the fog chamber and air supply are conditioned to be between 90% and 100% in RH with their respective humidifiers. The moist but unsaturated air minimizes LWC loss by evaporation of the fog droplets. Each test lasts

3 hours, after which any water remaining in the sinks are transferred to the respective containers and weighted on a balance. Meanwhile, any water collected inside the fog channel is weighted and deducted from the LWC outputted by the fog generator.

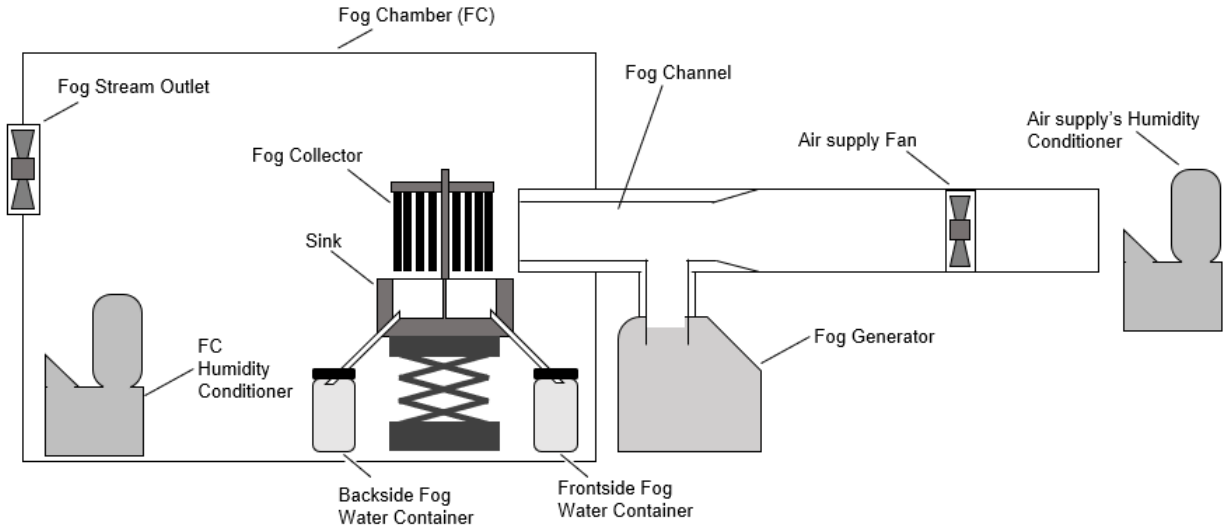

Figure 4.4 The experimental custom fog chamber used in the experiment with each component in its relative position. Figure is not drawn to scale.

CHAPTER 5: Performance and Optimization Discussion

Performance of the CFC is to be measured by the collection efficiency from *equation 3.1*. The collection efficiency at various shade coefficients, and surface wettability will be collected for optimization purpose. In addition, we will evaluate the water collection between the layers on the CFC.

5.1 CFC Collection Efficiency vs. Shade Coefficient

Two groups of CFCs are used to measures the changes in collection efficiency by shade coefficient. In the first group, we limit the column counts to 10 pieces per collector, but the columns' widths are different between collectors. The results from the first group will be used to verify the accuracy of the efficiency model by simultaneously changing the Stokes number and shade coefficient. For the second group, we limit the column's size to only 2.38mm wide, but no limit is placed on the number of columns per collector. The Stokes number is intentionally turned constant in group two, so the optimal shade coefficient for the CFCs can be located from the result. The shade coefficient for each model, and their respective theoretical collection efficiency are calculated using *equation 2.1, 2.2, and 3.2 – 3.6*. Each CFC model is placed into the fog chambers and tested for 3 times.

Table 5.1 The calculated shade coefficients (SC), and the corresponding theoretical collection efficiency ($\eta_{col,SC}$) and averaged experimental collection efficiency ($\eta_{col,exp}$) from group one with different copper tubes OD.

Copper Tubes OD (mm)	SC	$\eta_{Col,\ SC}$ (%)	$\eta_{Col,\ exp}$ (%)
1.59	0.27	5.51	3.13
2.38	0.40	5.40	3.96
3.18	0.53	4.81	2.84
3.97	0.68	3.76	2.70
4.76	0.78	2.65	3.18

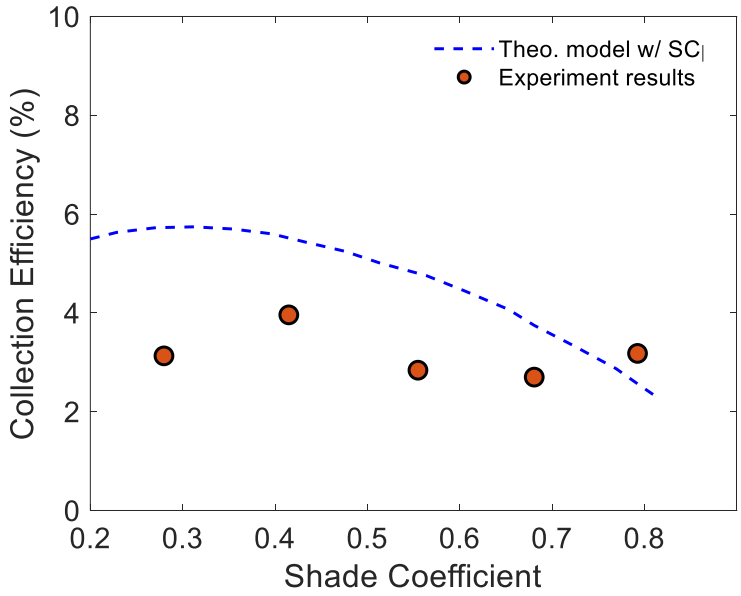

Figure 5.1 Group one's theoretical collection efficiency and the experimental results per shade coefficient. A mismatch on the shade coefficient for the maximum efficiency between the theoretical modal and the experimental values suggests the efficiency model need to be modified for the CFC.

In *figure 5.1*, group one's results disagrees strongly with the efficiency model on the optimal shade coefficient. Whereas the model predicts the peak efficiency at SC ≈ 0.3, we record the highest efficiency at SC ≈ 0.4. When reviewing footages of the experiments, we hypothesize a new geometry for A_{screen} and A_{op} from *equation 2.2* to account for the radial fog stream crossing the

CFC's surface (see *figure 5.2*). The efficiency model is recalculated using the new radial shade coefficient, SC^*, from the radial flow hypothesis, and compared to the experiment's data again (*figure 5.3*). The peak efficiency prediction at $SC^* \approx 0.3$ by the new efficiency model is on par with the experiment's results, proving the correctness of our hypothesis.

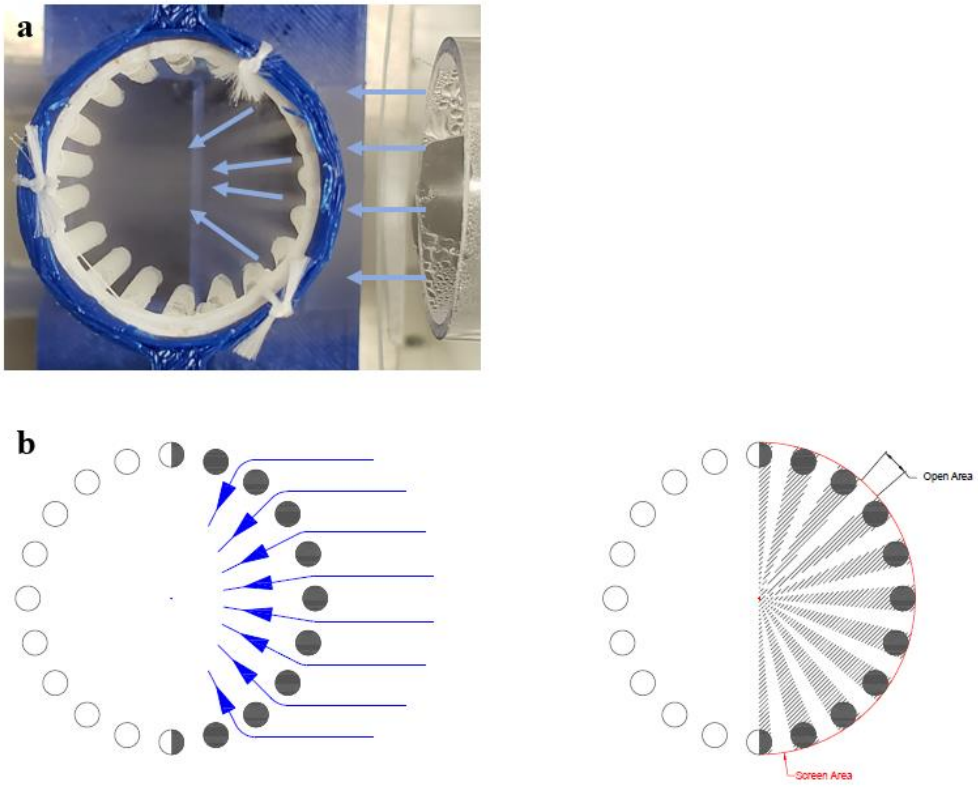

Figure 5.2 The new screen and open areas for the radial flow hypothesis. Based on (a) the fog's flow trajectories observed in our fog chamber, we hypothesize the flow's heading (b) as radially inward when connecting with the collector's surface and adjust the areas respectively.

Table 5.2 The radial shade coefficients (SC^*) based on the radial flow hypothesis, and the corresponding theoretical collection efficiency ($\eta_{col, SC}$) and averaged experimental collection efficiency ($\eta_{col,exp}$) from group one with different copper tubes OD.

Copper Tubes OD (mm)	SC*	η_{Col, SC^*} (%)	$\eta_{Col, exp}$ (%)
1.59	0.18	4.05	3.13
2.38	0.27	4.29	3.96
3.18	0.38	4.25	2.84
3.97	0.49	3.97	2.70
4.76	0.60	3.45	3.18

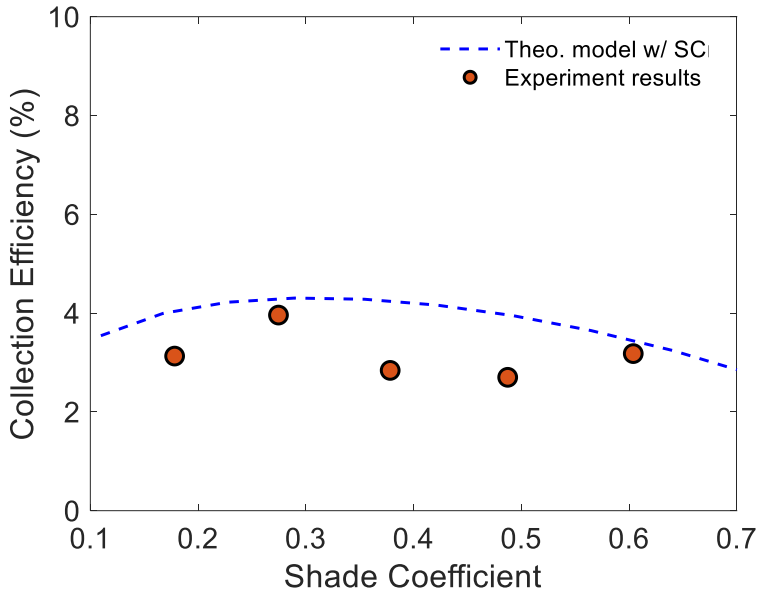

Figure 5.3 Group one's recalculated theoretical collection efficiency curve with SC^*. As compared to experiment's results, the new efficiency model agrees with the experimental value on an optimal $SC^* \approx 0.3$.

The optimal shade coefficient can be solved experimentally or numerically. The numerical solution of SC=0.55 has been solved for Raschel mesh and the fog harp. [31, 24] To testify the result for cylindrical collectors, we prepare 4 CFCs from group two for testing: BCU16, BCU20, BCU24, and BCU30 (*table 5.3*). The CFCs have 16, 20, 24, and 30 pieces of 2.38mm wide copper tubes respectively. The respective SC* for the cages are 0.44, 0.55, 0.66, and 0.82.

After performing the test thrice for each CFC, the average η_{col} is 4.53% for BCU16, 7.33% for BCU20, 6.61% for BCU24, and 5.49% for BCU30. The results (see *figure 5.4*) suggest the maximum η_{col} is likely located between $0.50 \leq SC^* \leq 0.60$, which matches with the theoretical value of 0.55. In addition, the results suggest that the CFCs are more efficient at fog harvesting at higher shade coefficient; but less so when the shade coefficient is less than optimal.

5.2 Wettability Modification

The superhydrophobic CFCs demonstrate superior effectiveness over the bare copper and superhydrophilic at all shade coefficient (*figure 5.4a*). At the optimal SC* = 0.55, HPO20 raises the collection efficiency by 0.78% (10% increase) over the unmodified BCU20. Surfaces of the superhydrophobic CFCs are densely populated by smaller spherical droplets which frequently coalesce with neighboring droplets (*figure 5.4c*). The coalescence of droplets instigates new droplets movement on the collector's surface, thus causing more coalescences, leading to a domino effect. The highly mobile droplets on the hydrophobic surface results in a shedding frequency twice of the unmodified copper surface and five times of the hydrophilic (*figure 5.4b*). Meanwhile, the superhydrophilic, HPI, samples have lower efficiency than the BCUs (*figure 5.4a*). Individual droplets cannot be seen on the hydrophilic surface, instead, a film of water covers the surface, and the excess water accumulates at the bottom of the columns forming large pendant drop. Based on the results, high droplet mobility is the most influential factor for increasing collection efficiency.

The effect of faster droplet shedding on superhydrophobic surface outweighs the strong attraction of water molecule in the fog by superhydrophilic surface.

Table 5.3 The shade coefficient and the static contact angle for modified superhydrophobically modified copper (HPO16~HPO30), unmodified bare copper (BCU16~BCU30), and modified superhydrophilically copper (HPI16~HPI30) cylindrical fog cage. In this test, all copper tubes have the same outer diameter (2.38mm), and the shade coefficient on each sample is changed by manipulating the tubes spacing.

Sample Cages	Shade Coefficient (SC)	Wettability	Static Contact Angle (degree)
HPO16	0.44	Superhydrophobic	165.0
HPO20	0.55	Superhydrophobic	165.0
HPO24	0.66	Superhydrophobic	165.0
HPO30	0.82	Superhydrophobic	165.0
BCU16	0.44	Neutral (Bare Copper)	114.7
BCU20	0.55	Neutral (Bare Copper)	114.7
BCU24	0.66	Neutral (Bare Copper)	114.7
BCU30	0.82	Neutral (Bare Copper)	114.7
HPI16	0.44	Superhydrophilic	9.9
HPI20	0.55	Superhydrophilic	9.9
HPI24	0.66	Superhydrophilic	9.9
HPI30	0.82	Superhydrophilic	9.9

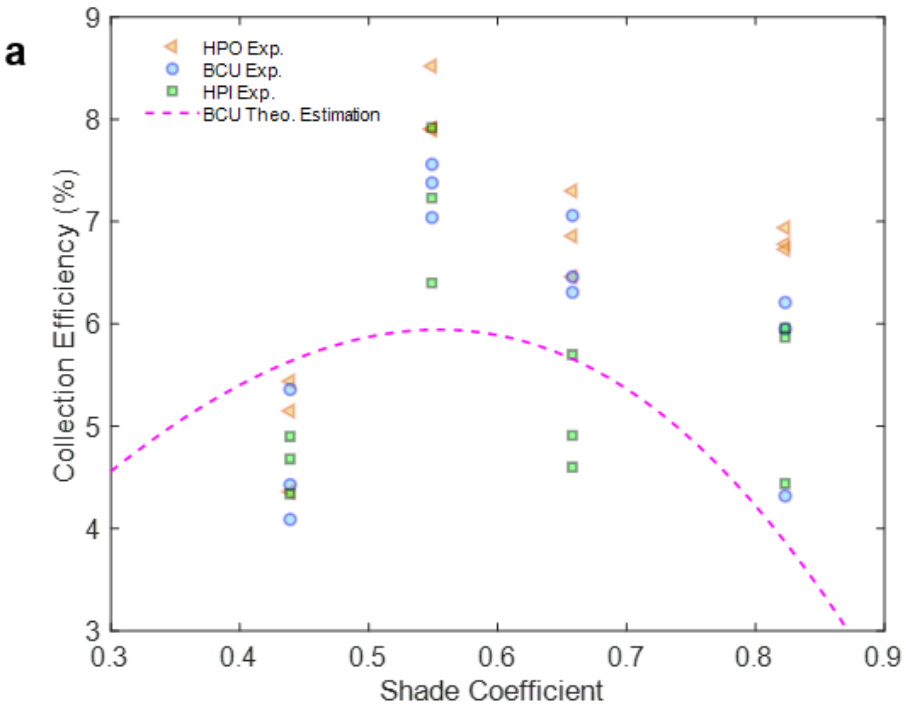
a
HPO Exp.
BCU Exp.
HPI Exp.
BCU Theo. Estimation
Collection Efficiency (%)
Shade Coefficient
9
8
7
6
5
4
3
0.3
0.4
0.5
0.6
0.7
0.8
0.9

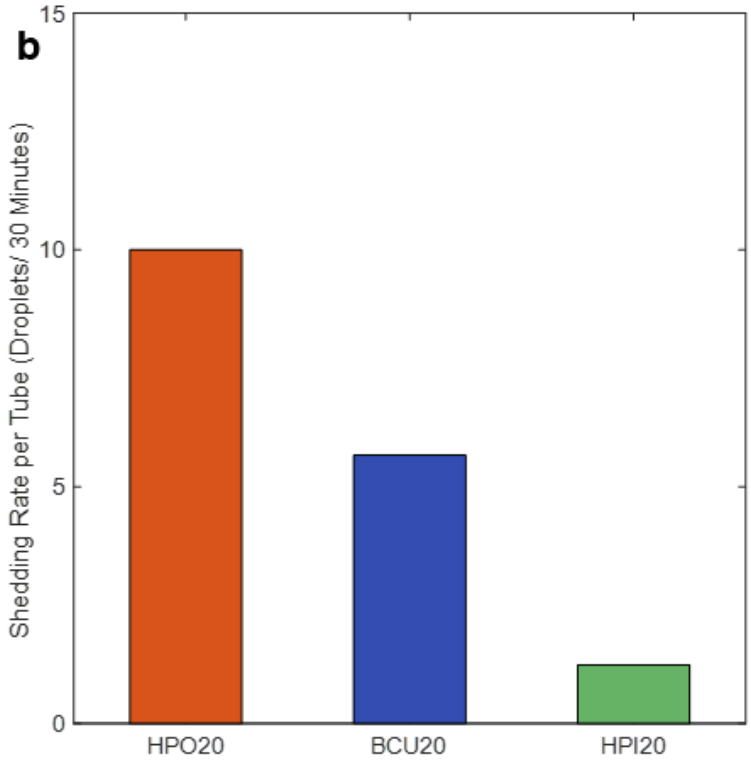
b
Shedding Rate per Tube (Droplets/ 30 Minutes)
15
10
5
0
HPO20
BCU20
HPI20

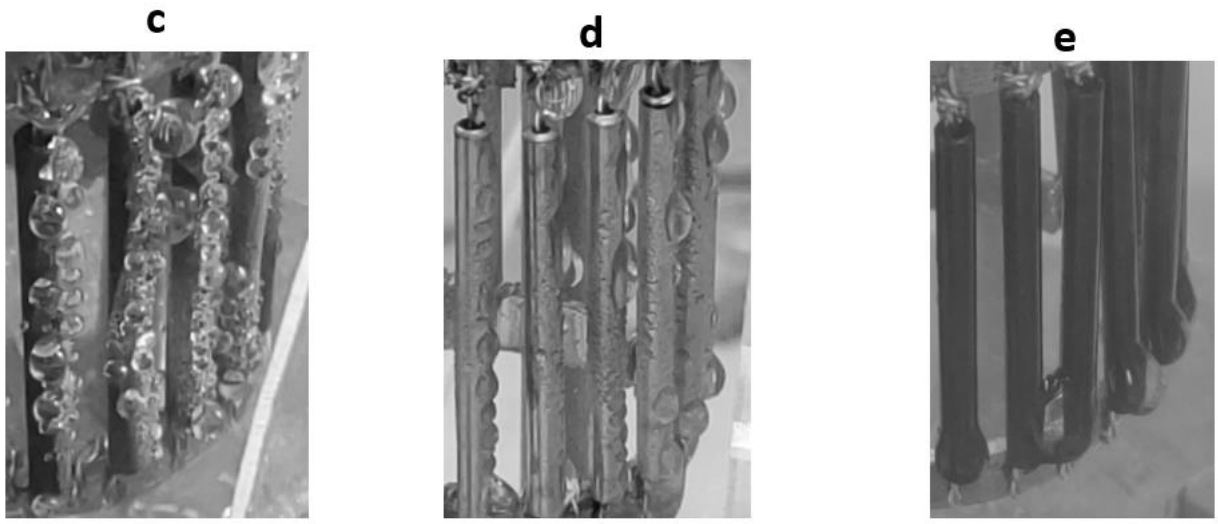

Figure 5.9 The cage fog collector's performance with various surface wetting. (a) Superhydrophobic surface demonstrates leading efficiencies over all SC. The concave down trend with maximum collection efficiency locating within $0.5<SC^{*}<0.6$ is observed in bare copper cages (BCU), and largely in superhydrophobic (HPO) and superhydrophilic (HPI) cages. (b) Droplets sheds at doubled rate after the copper tubes surface's wettability was modified to superhydrophobic. Droplets population is higher and denser on (c) superhydrophobic surface than (d) bare copper tubes. (e) A layer of water film is formed on the superhydrophilic surface. A single droplet grows on the bottom of each tube which may results in clogging the open channel upon coalescence.

5.3 Fog Water Collection by layer

The water capture between the two layers is shown in *figure 4.3*. Water collection by the trailing layer amounts to 0.55g on average by sample BCU16 during the 3 hours tests, equating to a 12% of the total water capture. The trailing collection diminishes quickly at higher SC as we record 0.28g, 0.02g, and 0.15g of fog water capture for BCU20, BCU24, and BCU30 respective. The minimal amount of water collection in the trailing layer can be explained by the reduced windspeed of the fog in middle of the CFC as shown in earlier simulations (*figure 3.2e to 3.2h*). At half of the unperturbed windspeed, the deposition efficiency of our system is reduced from 26% to 15%, hampering the collection efficiency. Meanwhile, the relatively larger contribution at lower

SC could possibly be related to the larger openings between the columns which allows more droplets to traverse the leading layer without affected by the column's boundary layers. In comparison to the multilayered harp studied by Azeem et al. [32], our study is inconclusive to determine whether the layered CFC has any noticeable advantage on fog collection efficiency other than completing the omnidirectional geometry. Our results suggest that optimizing the CFC as a single layered collector is more beneficial than attempting to maximize the efficiency of the second layer.

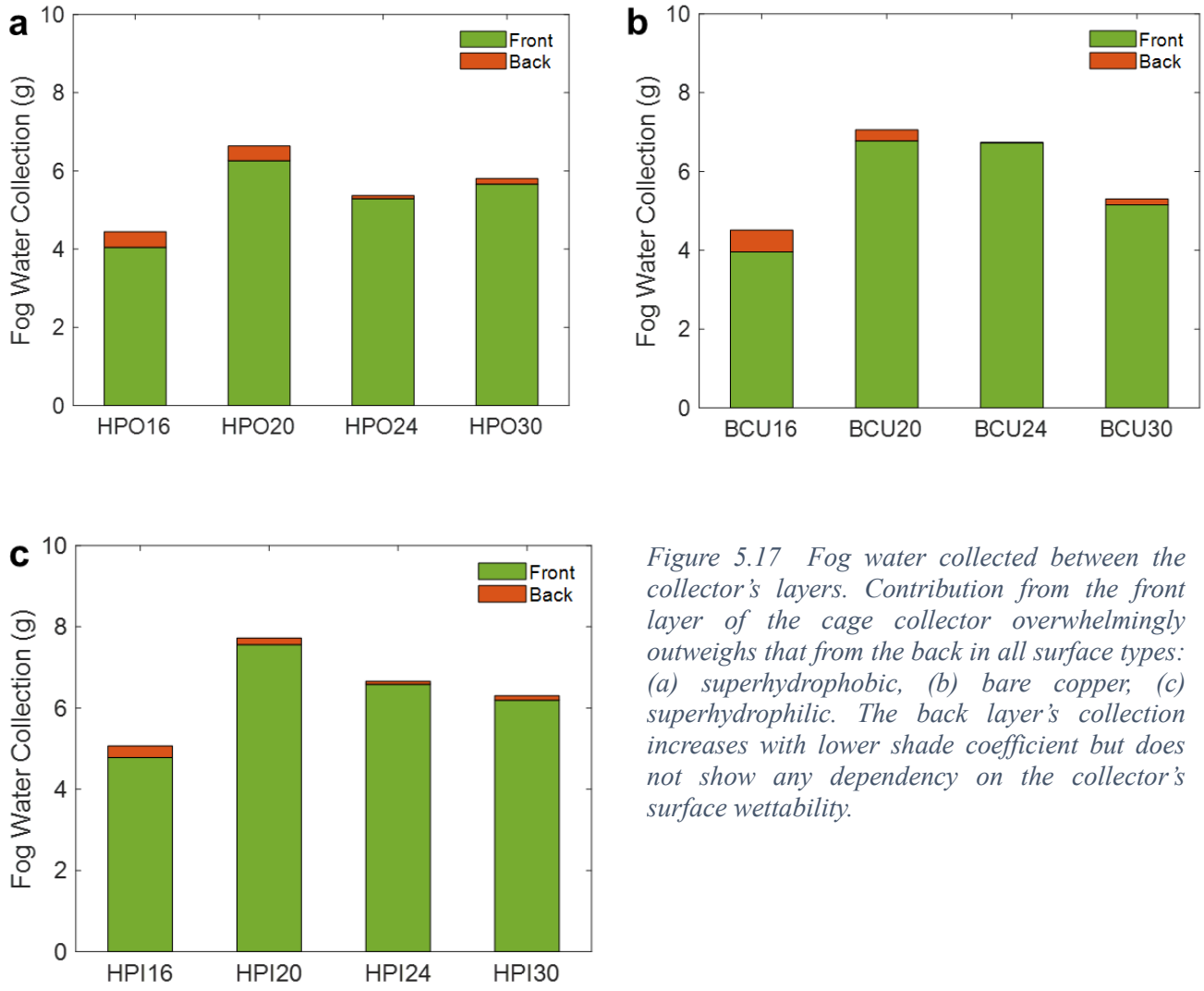

Figure 5.17 Fog water collected between the collector's layers. Contribution from the front layer of the cage collector overwhelmingly outweighs that from the back in all surface types: (a) superhydrophobic, (b) bare copper, (c) superhydrophilic. The back layer's collection increases with lower shade coefficient but does not show any dependency on the collector's surface wettability.

CHAPTER 6: CONCLUDING REMARKS

In this chapter, we summarize our designs, the performance, and optimization of the versatile cylindrical fog cage. We also share some challenges in our experiments, and our vision for future work to improve versatility of fog collectors.

6.1 Summary

In summary, we have introduced a versatile fog collector in a fully radial symmetric shape for fog harvesting in dynamic environment. The CFC will remain aerodynamically efficient at most direction thanks to a stable shade coefficient. The collection efficiencies of CFC have been evaluated, and the efficiency model refined for cylindrical fog collectors. The cage's optimal shade coefficient of 0.55 has been testified with experiments. We have also quantified the improvement on the CFC with hydrophobically modified copper surface. Finally, we review the possible cause to the lack-luster performance with the layered structure. In addition, we hypothesize that fog water capture is much more effective on the front layer of the CFC than the trailing layer because the flow slows down inside the cylinder, thus reduces the droplet's deposition efficiency according to the theoretical models. We hope that this study will inspire future research and development of different versatile fog collectors that ameliorates fog harvesting in dynamic weathers.

6.2 Challenges and Future Work

Simulating realistic fog is a tremendous challenge in laboratory. With an open system in particular, the humidity conditioning system is difficult to monitor because the microdroplets produced by the ultrasonic humidifier may contact the humidity probe and skew the reading. At the same time, microdroplets from the fog generator settle onto the pipe's inner surface along the path to the fog collector which make it difficult to account the actual loss of liquid water content due to condensates. It is also worth to mention that taking a quality snapshot of a flying

microdroplet for measurement is impossible without a highspeed camera with sufficient magnification.

In future studies, we plan to improve the versatility of the current design by tackling other dynamic challenges from nature, e.g. sudden change in wind speed, fluctuating droplets size, etc. Some design ideas may include, but not limited to, replacing the solid copper tubes with contractable fibers, giving the collector the ability to adjust the Stokes number for larger droplets The goal of the versatile design is to minimize any loss in the collection efficiency due to unpredictable natural events. Therefore, the collector will be readily deployable in any terrain and weather.

REFERENCES

[1] Y. Jiang, "China's Water Scarcity," *Journal of Environmental Management,* vol. 90, no. 11, pp. 3185-3196, 2009.

[2] D. Seckler, R. Barker and U. Amarasinghe, "Water Scarcity in the Twenty-first Century," *Int. Journal of Water Resources Development,* vol. 15, no. 2, pp. 29-42, 1999.

[3] UN-Water, "UN-Water Analytical Brief on Unconventional Water Resources," United Nations, 2020.

[4] T. Younis and K. Tulou, "Overview of Desalination Techniques," *Journal of Contemporary Water Research & Enducation,* no. 132, pp. 3-10, 2005.

[5] N. Tangsubkul, P. Veavis, S. Moore, S. Lundie and T. Waite, "Life Cycle Assessment of Water Recycling Technology," *Water Resources Management,* vol. 19, pp. 521-537, 2005.

[6] J. Groen, S. Ge and M. Pearson, "Offshore Fresh Groundwater as a Global Phenomenon," *Nature,* vol. 504, no. 7478, pp. 71-78, 2013.

[7] K. Kaseke and L. Wang, "Fog and Dew as Potable Water Resources: Maximizing Harvesting Potential and Water Quality Concerns," *GeoHealth,* vol. 2, pp. 327-332, 2018.

[8] J. Domen, W. Stringfellow, M. Camarillo and S. Gulati, "Fog Water As an Alternative and Sustainable Water Resource," *Clean Techn Environ Policy,* vol. 16, pp. 235-249, 2014.

[9] R. Schemenauer, R. Melissa and V. Carter, "Fog Collection Projects in Tojquia and La Ventosa, Guatemala.," in *4th Internal Conference on Fog, Fog Collection and Dew,* 2007.

[10] "Fog Harvesting," UN Climate Technology Centre & Network.

[11] R. Paul, S. Kenway and P. Mukheibir, "How scale and technology influence the energy intensity of water recycling systems-An analytical review," *Journal of Cleaner Production,* vol. 215, pp. 1457-1480, 2018.

[12] T. Asano and A. D. Levine, "Wastewater Reclamation, Recycling and Reuse: Past, Present, and Future," *Water Science and Technology,* vol. 33, no. 10-11, pp. 1-14, 1996.

[13] E. R. Jones, M. T. van Vliet, M. Qadir and M. F. Bierkens, "Country-level and gridded estimates of watewater production, collection, treatment and reuse," *Earth Syst. Sci. Data,* vol. 13, pp. 237-254, 2021.

[14] S. Dolnicar, A. Hurlimann and B. Grun, "What affects public acceptance of recycled and desalinated water?," *Water Research,* vol. 45, no. 2, pp. 933-943, 2011.

[15] A. Al-Karaghouli and L. L. Kazmerski, "Energy consumption and water production cost of conventional and renewable-energy-powered desalination processes," *Renewable and Sustainable Energy Reviews,* vol. 24, pp. 343-356, 2013.

[16] S. Bunch, K. Cort, E. Johnson and D. Elliott, "Water and Wastewater Annual Price Escalation Rates for Selected Cities across the United States," US Department of Energy Office of Energy Efficiency & Renewable Energy, 2017.

[17] C. S. Mandal, M. Agarwal, V. Reddy and V. K. Kudapa, "Water from air-A sustainable source of water," *materialstoday:Proceedings,* vol. 46, pp. 3352-3357, 2021.

[18] R. Schemenauer and Cereceda P., "A Proposed Standard Fog Collector for Use in High Elevation Regions," *Journal of Applied Meteorology,* vol. 33, no. 11, pp. 1313-1322, 1994.

[19] K. Park, S. S. Chhatre, S. Srinivasan, R. Cohen and G. McKinley, "Optimal Design of Permeable Fiber Network Structures for Fog Harvesting," *Langmuir,* vol. 29, no. 43, pp. 13269-13277, 2013.

[20] O. Klemm, R. S. Schemenauer, A. Lummerich, P. Cereceda, V. Marzol, D. Corell, J. van Heerden, D. Reinhard, T. Gherezghiher, J. Olivier, P. Osses, J. Sarsour, E. Frost, M. J. Estrela, J. A. Valiente and G. M. Fesseheya, "Fog as a Fresh-Water Resource: Overview and Perspectives," *Ambio.,* vol. 41, no. 3, pp. 221-234, 2012.

[21] . J. Knapczyk-Korczak, P. K. Szewczyk, D. P. Ura, . K. Berent and U. Stachewicz, "Hydrophilic Nanofibers in Fog Collectors for Increased Water Harvesting Efficiency," *RSC Advances,* vol. 10, no. 38, pp. 22335-22342, 2020.

[22] J. d. D. Rivera and D. Lopez-Garcia, "Mechanical Characteristics of Raschel Mesh and Their Application to the Design of Large Fog Collectors," *Atmospheric Research,* vol. 151, pp. 250-258, 2015.

[23] W. Shi, L. H. De Koninck, B. J. Hart, N. G. Kowalski, A. P. Fugaro, T. W. van der Sloot, R. S. Ott, B. S. Kennedy and J. B. Boreyko, "Harps under Heavy Fog Conditions: Superior to Meshes but Prone to Tangling," *ACS Appl Mater Interface,* vol. 12, no. 42, pp. 48124-48132, 2020.

[24] W. Shi, M. Anderson, J. Tulkoff, B. Kennedy and J. Boreyko, "Fog Harvesting with Harps," *ACS Appl. Mater. Interfaces,* vol. 10, no. 14, pp. 11979-11986, 2018.

[25] J. Park and S. Kim, "Three-Dimensionally Structured Flexible Fog Harvesting Surface Inspired by Namib Desert Beetles," *Micromachines,* vol. 10, no. 3, p. 201, 2019.

[26] Y. Tian, P. Zhu, X. Tang, C. Zhou, Wang J., T. Kong, M. Xu and L. Wang, "Large Scale Water Collection of Bioinspired Cavity Microfibers," *National Communications,* vol. 8, no. 1, 2017.

[27] V. Sharma, R. Balaji and V. Krishnan, "Fog Harvesting Properties of Dryopteris Marginata: Role of Interscalar Microchannels in Water-Channeling," *Biomimetrics,* vol. 3, no. 2, p. 7, 2018.

[28] R. Schemenauer and P. Joe, "The Collection Efficiency of a Massive Fog Collector," *Atmospheric Research,* no. 24, pp. 53-69, 1989.

[29] C. Regalado and A. Ritter, "The Design of an Optimal Fog Water Collector: A Theoretical Analysis," *Atmospheric Research,* Vols. 178-179, pp. 45-54, 2016.

[30] D. Rader and A. Geller, "Transport and Deposition of Aerosol Particles," in *Developments in Surface Contanmination and Cleaning Vol.1: Fundamentals and Applied Aspects,* R. Kohli and K. L. Mittal, Eds., San Diego, California: Matthew Deans, 2008, pp. 23-90.

[31] J. Rivera, "Aerodynamic Collection Efficiency of Fog Water Collector," *Atmospheric Research,* vol. 102, no. 3, pp. 335-342, 2011.

[32] M. Azeem, A. Guerin, T. Dumais, L. Caminos, R. Goldstein, A. Pesci, J. Rivera, M. Torres, J. Wiener, J. Campos and J. Dumais, "Optimal Design of Multilayer Fog Collectors," *ACS Appl. Mater. Interfaces,* vol. 12, pp. 7736-7743, 2020.

[33] D. Seo, J. So, W. Bae and Y. Won, "The Design of Hydropholic Nanochannel-Macrostripe Fog Collector: Enabling Wicking-Assisted Vertical Liquid Delivery for the Enhancement in Fog Collection Efficiency," *Adv. Mater. Interfaces,* vol. 7, no. 11, p. 1902150, 2020.

[34] P. Dubey, H. Cho, Q. Pham, Y. Kim and Y. Won, "Controlled Wetting Properties through Heterogeneous Surface Containing Two-level Nanofeatures," *ACS Omega,* vol. 2, pp. 7916-7922, 2017.